

Boise State University

ScholarWorks

Materials Science and Engineering Faculty
Publications and Presentations

Micron School for Materials Science and
Engineering

9-7-2021

First-Principles Magnetic Treatment of the Uranium Nitride (100) Surface and Effect on Corrosion Initiation

Ember L. Sikorski
Boise State University

Brian J. Jaques
Boise State University

Lan Li
Boise State University

This article may be downloaded for personal use only. Any other use requires prior permission of the author and AIP Publishing. This article appeared in Sikorski, E.L.; Jaques, B.J.; & Li, L. (2021). First-Principles Magnetic Treatment of the Uranium Nitride (100) Surface and Effect on Corrosion Initiation. *Journal of Applied Physics*, 130(9), 095301. and may be found at <https://doi.org/10.1063/5.0056904>.




First-principles magnetic treatment of the uranium nitride (100) surface and effect on corrosion initiation

Cite as: J. Appl. Phys. **130**, 095301 (2021); doi: [10.1063/5.0056904](https://doi.org/10.1063/5.0056904)

Submitted: 15 May 2021 · Accepted: 22 July 2021 ·

Published Online: 1 September 2021



Ember L. Sikorski,^{1,2}  Brian J. Jaques,^{1,2}  and Lan Li^{1,2,a)} 

AFFILIATIONS

¹Micron School of Materials Science and Engineering, Boise State University, Boise, Idaho 83625, USA

²Center for Advanced Energy Studies, Idaho Falls, Idaho 83401, USA

^{a)}Author to whom correspondence should be addressed: lanli@boisestate.edu

ABSTRACT

The magnetic properties of uranium nitride (UN) surfaces are not well understood experimentally or computationally but they have a significant effect on UN performance as a nuclear fuel. We investigated ferromagnetic (FM), antiferromagnetic (AFM), nonmagnetic (NM), and three hybrid magnetic structures of the most stable UN surface (100). To account for electron correlation and metastability, a U-ramp was performed to an effective Hubbard U-term of 2.0 eV. FM was found to be the most energetically favorable magnetic structure. Type 1 AFM slab was optimized to a new magnetic structure consisting of (100) planes with either all spin-up electrons, all spin-down electrons, or half spin-up and half spin-down electrons on uranium atoms. After OH adsorption to simulate corrosion initiation, the AFM, FM, and NM structures yield relatively similar bond lengths but varying bond angles, adsorption energies, and electronic profiles. Partial charge density maps show varying degradation mechanisms across magnetic structures. Electron localization function reveals more charge localized to AFM uranium atoms with spin-down electrons than uranium atoms with spin-up electrons. This leads to different properties depending on if an adsorbate interacts with a spin-up or spin-down terminated AFM surface. This work supports the physical accuracy of future computational studies toward corroborating with experiments and addressing UN fuel corrosion.

Published under an exclusive license by AIP Publishing. <https://doi.org/10.1063/5.0056904>

I. INTRODUCTION

Uranium nitride (UN) is proving to be a promising candidate for nuclear fuel due to its high actinide density, thermal conductivity, and melting point.^{1–3} One barrier for implementation is its instability in the presence of water. Several experimental^{4–8} studies have sought to determine the mechanism of UN corrosion, though there is not yet a consensus on the chemical reactions that occur. Dell *et al.*⁴ first proposed the UN corrosion mechanism as $\text{UN} + 2\text{H}_2\text{O} \rightarrow \text{UO}_2 + \text{NH}_3 + \frac{1}{2}\text{H}_2$. However, Dell *et al.* noted that there was dissolved N as well as a U_2N_{3+x} phase in the corrosion product. Subsequent experimental studies have continued to report the presence of UN_2 , U_2N_3 , and/or residual N in the product.^{5–8} This suggests that the initially proposed corrosion mechanism is incomplete in the hypothesis that all N is converted into NH_3 . To complement experimental studies, Density Functional Theory (DFT) has been a common method used to

study UN surfaces exposed to H_2O or O_2 at the atomic scale.^{9–14}

While experimental studies might utilize UN reactants of varying density, purity, and geometries, DFT allows for precise selection of the reactant. Though DFT calculations occur at 0 K, its precise reactant selection as well as further investigation of atomic corrosion initiation mechanisms capabilities make it a vital strategy for improving the understanding of UN corrosion.

However, these DFT studies have applied different magnetic structures to the UN surface. This variation in the magnetic treatment of the surface might significantly affect the simulations, highlighting the uncertainty of prediction of the chemical reactions occurring during the corrosion. As we develop our understanding of UN corrosion, the effect of the magnetic structure on such properties should be further investigated. Additionally, without agreement upon the magnetic structure, DFT data could be translated to inaccurate descriptions of larger length scale phenomena.

The variations in magnetic treatments to UN surfaces in DFT studies stem from disagreement over whether a UN surface has the same magnetic structure as UN bulk. In bulk, UN is type 1 antiferromagnetic (AFM) below the Néel temperature (approximately 53 K),² such that (100) planes alternate between positive and negative spin.¹⁵ However, it has been observed in DFT studies that for UN slabs, typically ranging from 3 to 11 monolayers (approximately 7–27 Å), the ferromagnetic (FM) structure is more stable than the AFM structure.^{2,9,16,17} Likewise, FM treatment has yielded more energetically favorable adsorption energies.¹⁸ However, these studies have not included the Hubbard U-term in their magnetic consideration. In traditional DFT, electrons are systematically delocalized, which can lead to inaccurate descriptions for strongly correlated materials including actinides.¹⁹ These descriptions can be improved with the incorporation of a Coulomb repulsion U-term for f electrons following the ideas of Hubbard.^{20,21} For UN, it has been found necessary to include the U-term in DFT calculations to reproduce lattice parameter, bulk modulus, phonon properties, magnetic structure, and magnetic moment in good agreement with experiments.^{22,23} Gryaznov *et al.* showed that as the U-term was increased, the most stable UN bulk magnetic structure transitioned from FM to AFM above an effective U-term, U_{eff} of 1.65 eV.²³

Three different strategies have been reported for treating the UN surface magnetic structure in the DFT calculations. Bo *et al.* used AFM treatment in order to replicate the most stable magnetic structure of the bulk.¹³ Li *et al.* suggested that nonmagnetic treatment was appropriate for only total energy calculations.¹¹ Most prevalently, a few studies used FM treatment,^{10,14,18,24} citing FM as the most energetically favorable structure. In experiments, Rafaja *et al.* studied the magnetic susceptibility of reactive sputtered UN thin films, suggesting FM for UN crystallites (averaging 17 nm).²⁵ Bright *et al.* studied an epitaxial UN film (70 nm) using x-ray synchrotron techniques and reported an AFM structure.²⁶ However, both experimental studies treated thicker UN systems (over 100 Å thicker) than the DFT studies did.

In our previous work, we studied UN (100) and (110) surfaces using DFT.¹⁴ In agreement with Tasker's analysis²⁷ and other DFT studies,^{11,12} we found the (100) surface to be the most energetically favorable. In order to comprehensively understand the magnetic structure of UN and its surface effect, this work investigates three key aspects. First is to identify the most stable magnetic structure of UN (100) in consideration with the Hubbard U-term. Second is to evaluate if a transition between FM and AFM structure is favorable. Final is to determine the effects of different magnetic structures on bond lengths, bond angles, adsorption energies, and electronic mapping.

II. METHODS

DFT calculations were performed using the Vienna *Ab Initio* Simulation Package (VASP).²⁸ Spin-polarized generalized gradient (GGA) exchange-correlation functional was used with the Perdew–Burke–Ernzerhoff (PBE) formulation.²⁹ Plane-wave basis sets were implemented utilizing projector-augmented wave (PAW) pseudo-potentials. Simulations were performed with a cutoff energy of 550 eV and $4 \times 4 \times 1$ gamma-centered k-points.

UN slabs were constructed with eight monolayers and a surface area of 16 atoms, i.e., the UN unit cell was extended by factors of $2 \times 2 \times 4$ to form supercells. In our previous work, we found trends in electronic mapping to be converged for four monolayers, but binding energies varied between four and eight monolayer systems by up to approximately 0.5 eV.¹⁴ Similarly, Bocharov *et al.* found defect energies to be converged for slabs with seven or more monolayers.²⁴ Bo *et al.* compared defect energies, surface energies, and bond lengths between supercells with surface areas corresponding to 2×2 and 3×3 unit cells and found the 2×2 surface area to be sufficient for corrosion studies.¹³

The U-term was applied using the Dudarev implementation to better treat the f electrons of U.¹⁹ In this version, only the effective U-term, $U_{\text{eff}} = U - J$, between the Hubbard U and exchange parameter J is considered. The J parameter was fixed at 0.5 eV and the U parameter was varied to reach the desired U_{eff} . While the U-term improves the DFT description of actinides, it introduces an additional concern of converging to metastable states.³⁰ As such, calculations may not always reach the global energetic minima, which can lead to errors in the calculations. The so-called “U-ramping” method is one technique that has been developed to better find the ground state.³¹ In this method, U_{eff} is gradually increased from zero to the desired value in increments of 0.1 eV. For each step, the previous atomic coordinates and wave functions are used as the initial guess for a new calculation.

Gryaznov *et al.* showed that the stable magnetic structure of the UN bulk, either FM or AFM, depended on the U_{eff} value. Therefore, we performed a U-ramp on the UN (100) slabs to not only treat the metastability but also survey the most favorable magnetic structure over a range of U_{eff} values. Previous UN corrosion studies used a U_{eff} value of 1.9 eV.^{12–14} This value could balance the 1.85 eV recommendation from Gryaznov *et al.*²³ for magnetic properties and the recommendation of 2.0 eV from Lu *et al.*²² for lattice parameter, bulk modulus, and phonon properties. To encompass all these recommended U_{eff} values, the U-ramp was performed up to 2.0 eV in our studies. While the incorporation of spin-orbit coupling (SOC) can reduce the magnetic moment and increase the U_{eff} at which the magnetic transition occurs,²³ previous first-principles UN studies have not included SOC due to the low amplitude of improvement,²² negligible effect on electronic and geometric properties,¹¹ and unknown effect on point defect energies.³² Incorporating SOC only shifts the U_{eff} transition from AFM to FM favorability for bulk UN by 0.15 eV.²³ Since we have surveyed the full range of recommended U_{eff} values for UN, we have not included SOC and do not expect it will change our findings on magnetic structure favorability.

During the U-ramp, slabs were relaxed symmetrically, i.e., the center two monolayers were fixed, to prevent any unphysical polarity from affecting the favorability of each magnetic structure. Optimization of a single OH adsorbate in the $2 \times 2 \times 4$ UN (100) supercell, i.e., 1/8 adsorbate to U atom surface coverage, was performed. The bottom two layers of the UN slab were fixed to simulate the bulk region. Since our previous work demonstrated the sensitivity of adsorption energy to slab thickness,¹⁴ asymmetric surface relaxation was utilized to ensure adsorption energy accuracy.

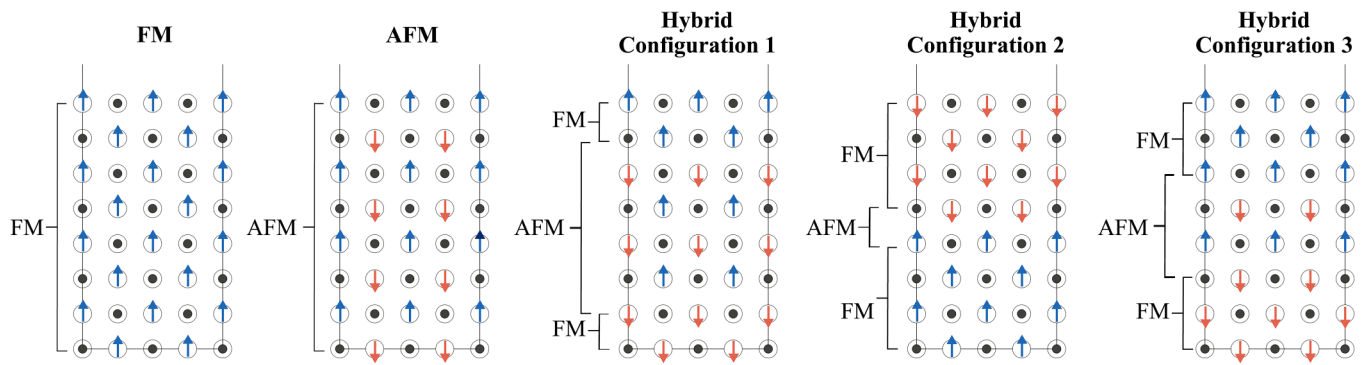


FIG. 1. Initial magnetic structures applied during U-ramp to $U_{\text{eff}} = 2.0$ eV. Arrows correspond to the spin applied to the U atom electrons.

III. RESULTS

A. Magnetic structure

With bulk UN exhibiting the AFM structure and surfaces exhibiting the FM structure, it would be crucial to determine a transition mechanism from AFM to FM. We tested AFM, FM, and another three possible hybrid magnetic structures for comparison, as seen in Fig. 1. Using symmetrical slabs, the central layers represent the bulk and as such, we applied the AFM structure of varying thicknesses for the hybrid configurations. Hybrid Configuration (HC) 1 has the greatest AFM character with six central AFM monolayers, leaving two FM monolayers at each terminating surface. HC2 has only two central AFM monolayers with four FM monolayers on either side. HC3

has four central AFM layers and three FM monolayers on either side.

For each magnetic structure, we performed a U-ramp to 2.0 eV, which included the recommended values to accurately reproduce UN bulk magnetism, lattice parameter, bulk modulus, and phonon properties.^{22,23} Figure 2 shows the relative energies for each magnetic structure with reference to the most energetically favorable magnetic structure (FM) during the U-ramp. Without the U-term (i.e., $U_{\text{eff}} = 0$ eV), FM is the most stable while AFM is the least stable, in agreement with Zhukovskii *et al.*^{16,17} and Evarestov *et al.*³³ Before the U-ramp, FM is more stable than AFM by 2.66 eV. For the duration of the U-ramp, FM remains the most stable magnetic structure, unlike bulk UN that would transition from FM to AFM at $U_{\text{eff}} = 1.65$ eV.²³ There are a couple of transitions of the order of the magnetic configuration stability of the HC structures. At $U_{\text{eff}} = 1.6$ eV, HC1 becomes more stable than HC3. At $U_{\text{eff}} = 2.0$ eV, HC1 becomes more stable than HC2. At $U_{\text{eff}} = 2.0$ eV, the magnetic structures from the most to the least stable are FM, HC1, HC2, HC3, and AFM.

Except for AFM, the initial magnetic structures (Fig. 1) are maintained for the duration of the U-ramp, as shown in Table I. FM, HC1, HC2, and HC3 exhibit that the magnitudes of the magnetic moments in layers 1–4 mirror those in layers 5–8. The higher magnitudes of the magnetic moments occur in the outer layers 1

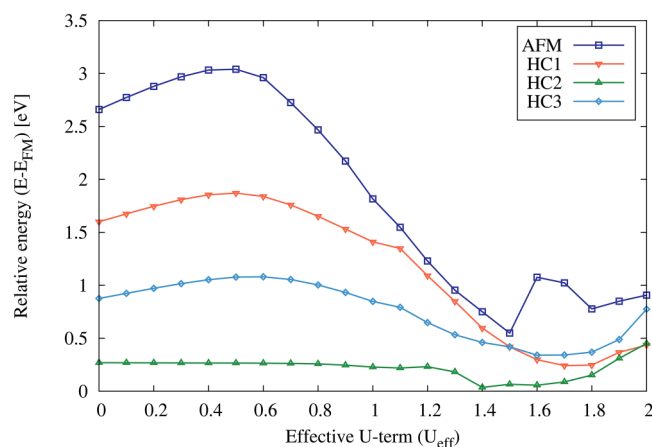


FIG. 2. Relative energy (eV) of the magnetic structures with respect to U_{eff} during the U-ramp to 2.0 eV. Energies are given with respect to the FM total energy at each respective U_{eff} value. Note that the AFM values correspond to the structure that was initialized as type 1 AFM, corresponding to bulk UN, before the U-ramp but transitioned to a new magnetic structure as shown in Table I.

TABLE I. Magnetic moments (μ_B) of U atoms averaged over each (100) layer after U-ramping to $U_{\text{eff}} = 2.0$ eV.

	FM	AFM	HC1	HC2	HC3
Layer 1	2.10	−2.07	−2.11	2.09	2.07
Layer 2	1.93	1.46	−1.79	1.89	1.85
Layer 3	1.79	0.01	1.89	1.75	1.47
Layer 4	1.72	1.69	−1.72	1.57	−1.80
Layer 5	1.74	0.42	1.84	−1.52	1.80
Layer 6	1.75	−1.26	−1.68	−1.76	−1.47
Layer 7	1.89	−0.07	1.77	−1.89	−1.85
Layer 8	2.10	−0.01	2.09	−2.09	−2.07

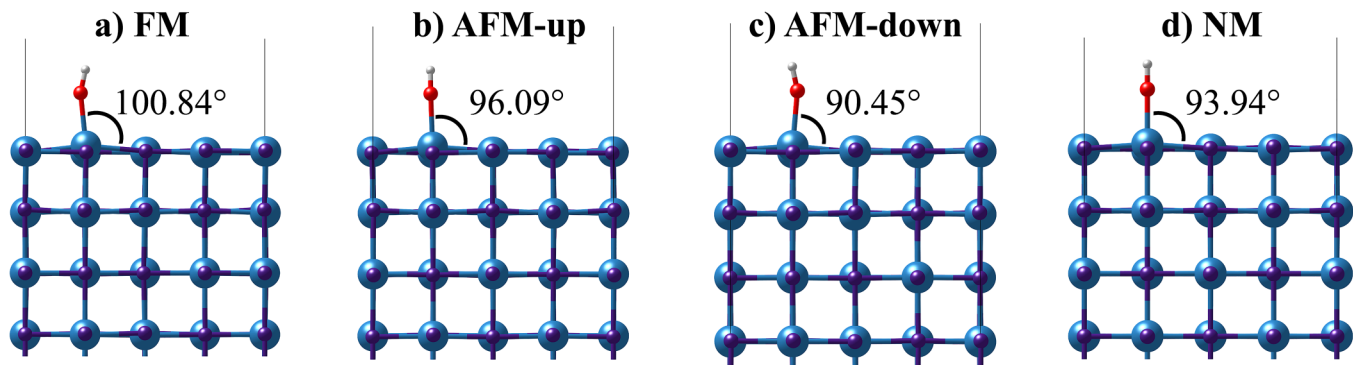


FIG. 3. Atomic structures after OH adsorption for (a) FM, (b) AFM spin-up terminated, (c) AFM spin-down terminated, and (d) NM structures. Blue, purple, red, and white atoms represent U, N, O, and H, respectively.

and 8 and gradually decrease moving toward the central layers 4 and 5. Conversely, for AFM, some of the electrons of the U atoms flip their spins at $U_{\text{eff}} = 1.6$ eV in layers 3, 5, 7, and 8. Layers 3, 5, and 7 started as spin-down and the electrons of half of the U atoms flipped to spin-up. Layer 8 started as spin-up and half of the electrons of the U atoms flipped to spin-down. This results in layers 3, 5, 7, and 8 exhibiting internal AFM structures with half the U atoms with spin-up electrons and half with spin-down electrons. At the end of the U-ramp ($U_{\text{eff}} = 2.0$ eV), this new AFM structure is less stable than the FM structure by 0.91 eV.

B. Electronic structure

To understand the effect of magnetic structures on corrosion results, we relaxed OH at the U-top site of the three magnetic structures used in the literature: FM, AFM, and NM, as seen in Fig. 3. OH serves as a critical step in corrosion at UN surfaces in the first-principles UN studies.^{12–14,18} OH adsorption is most favorable at the U-top site.¹² In order to determine the effect of electron-spin polarization on adsorption properties, OH was studied at both AFM spin-up and spin-down terminated surfaces. The most readily apparent difference in OH adsorption across structures is the variation in O–U–N bond angles. Additional bond angles as well as bond lengths, vertical displacement of the U atoms bonded to O, and adsorption energies are given in Table II.

All the magnetic treatments yield identical O–H and O–U bond lengths, except for NM, which yields a 0.05 Å shorter O–U bond length. The H–O–U bond angles are obtuse for the spin-polarized structures and vary at most by 1.67°, while NM yields a 180° bond angle. The O–U–N bond angles vary significantly more across spin-polarized structures with differences up to 10.39°. FM predicts a U displacement of 0.39 Å, while NM underpredicts the displacement by 0.19 Å and both AFM structures overpredict the displacement by at least 0.20 Å. NM predicts the greatest magnitude of adsorption energy, FM the smallest, and both AFM structures lie in the middle.

The Local Densities of States (LDOS) for OH adsorbed on the FM, AFM, and NM slabs, shown in Fig. 4, depict relatively similar trends. Valence and conduction electrons are localized primarily on U and N. More electrons are localized on N than U from approximately –6 to –2 eV, while more electrons are on U than N from approximately –2 to 2 eV. Hybridization of O with U and N occurs around –4 eV.

Partial Charge Densities (PCDs) for OH adsorbed on the FM, AFM, and NM slabs are shown in Fig. 5. PCD can project the electronic states of interest onto individual atomic sites, providing further insight into electronic profiles. The electronic states of –6 eV to the Fermi energy, which capture the majority of the bonding between U, N, and O atoms (Fig. 4), are shown for each magnetic structure in Figs. 5(a)–5(c). For each structure, valence electrons are localized to U, N, and the adsorbed O. To better

TABLE II. Bond lengths, bond angles, vertical displacement of the U atom bonded to OH after geometry optimization, and adsorption energy for FM, AFM spin-up terminated, AFM spin-down terminated, and NM magnetic structures. Two O–U–N bond angles are reported for each structure: one considering the neighboring N atom pictured to the right and one considering the N atom into the page in Fig. 3.

	O–U bond length (Å)	O–H bond length (Å)	H–O–U bond angle (°)	O–U–N right angle (°)	O–U–N into page angle (°)	U displacement (Å)	Adsorption energy (eV)
FM	2.17	0.97	162.05	100.84	95.65	0.39	–4.41
AFM-up	2.17	0.97	163.72	96.09	100.64	0.62	–4.56
AFM-down	2.17	0.97	162.82	90.45	96.17	0.60	–4.83
NM	2.12	0.97	180.00	93.94	93.94	0.20	–5.23

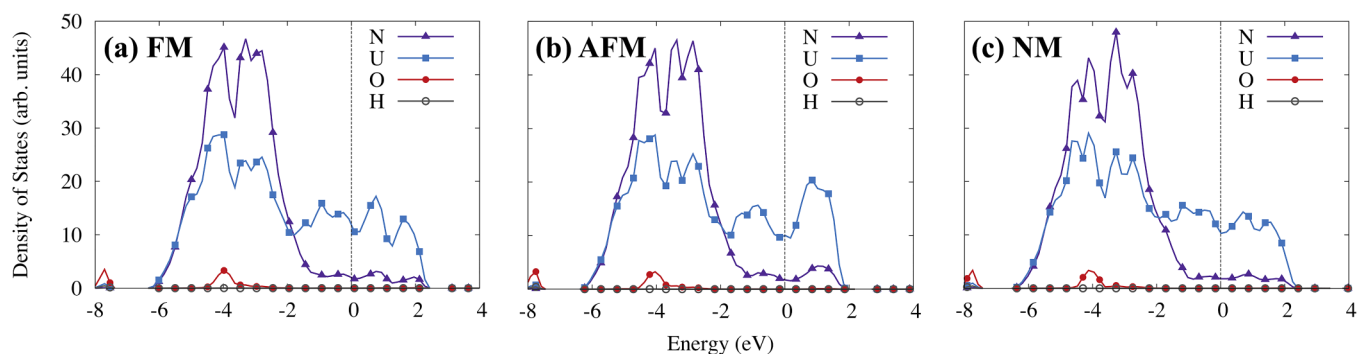


FIG. 4. Local densities of states for OH relaxed on (a) FM, (b) AFM, and (c) NM slabs. The Fermi energy is shifted to 0 eV.

discern variations in bonding across structures, the mapped electronic states are narrowed to the valence electrons from -2 eV to the Fermi energy in Figs. 5(d)–5(f). Across structures, valence electrons are more localized to U atoms than N atoms in this energy range. Covalent bonds between the terminating layer of the UN surface and the second layer become weaker in comparison to those in the bulk region. This is evident in the narrower contour regions between U1 and the rest of the U and N atoms. In the FM structure, U1 remains covalently bonded to N1 and N2 as well as U3. However, the bond between U1 and U2 is greatly weakened, shown by the disappearance of the connecting contoured region. In

contrast, in AFM, U1 remains bonded to N2, U2, and U3, while its bond with N1 is greatly weakened. In NM, while the contoured regions between U1 and its neighboring N and U atoms are weakened as compared to the bulk, none of them are weakened to the same extent as in both FM and AFM.

Electron Localization Function (ELF) analysis can further reveal the overall electron localization, as shown in Fig. 6. Across structures, the electronic profile around the OH adsorbate is relatively similar with the majority of charge localized to H and additional charge below the O. In the FM and NM structures, electrons are equally localized between the N and U atoms of the bulk. In

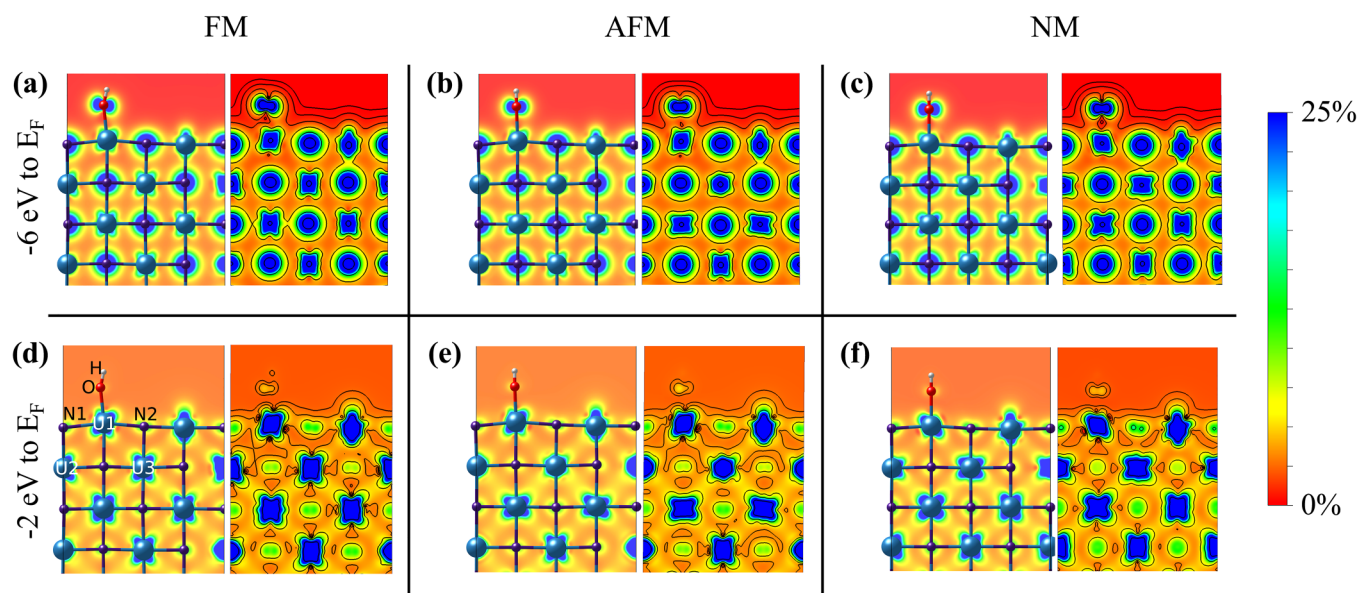


FIG. 5. Partial charge densities for OH adsorbed to FM, AFM, and NM magnetic structures. Valence electrons are shown from [(a)–(c)] -6 eV to the Fermi energy and from [(d)–(f)] -2 eV to the Fermi energy. The scale has been narrowed to 25% of the total electronic states to improve the visibility of bonds. Contour lines indicate areas with the same energy and are consistent across structures. Blue and red colors indicate many and no electronic states, respectively. Some U and N atoms have been numbered for reference in the text. The numbering scheme is consistent across magnetic structures.

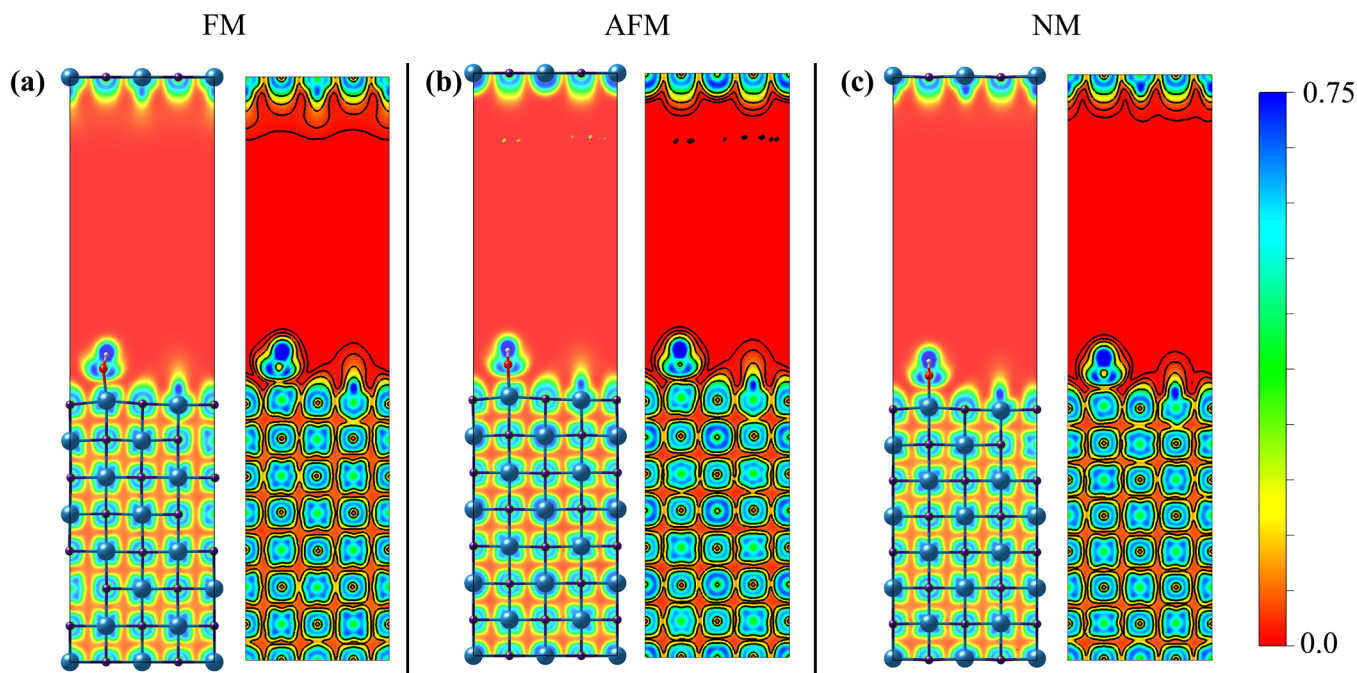


FIG. 6. Electron Localization Function (ELF) of OH adsorbed to (a) FM, (b) AFM, and (c) NM UN surfaces. The ELF is mapped such that 1 indicates a high probability of finding an electron, 0.5 is equivalent to the probability in a homogeneous electron gas, and 0 indicates a low probability.³⁴ Blue and red colors indicate high and low probability of finding a localized electron, respectively. Contour lines indicate areas with the same energy and are consistent across structures.

contrast, in the AFM structure, more electrons are localized to the U atoms with spin-down electrons than the other U atoms and N atoms. This reveals that OH adsorption properties on AFM surfaces could vary, depending on if the OH is adsorbed to a spin-up or spin-down terminated surface. Due to the periodic boundary conditions, both sides of each slab reveal electronic characteristics of the surface. By examining the top of the ELF, we can compare the electronic profiles of the pristine surfaces without OH interaction. In the FM structure, the iso-energy contour lines on the pristine surface side reveal a smooth, periodic electronic profile. In the AFM structure, there is unphysical charge build-up below the pristine surface, not localized to any atoms. Such charge build-up might occur in slab calculations with insufficient vacuum space to prevent interactions between slab images. However, the lack of such a charge in the FM and NM structures suggests that the vacuum length is sufficient. This charge build-up in the AFM structure might then be attributed to its metastability. The iso-energy contour lines on the NM pristine surface are not as smooth as that of the FM structure but there is no unphysical charge localization like the AFM structure.

IV. DISCUSSION

In bulk UN, a Hubbard U-term of at least 1.65 eV is required to yield AFM as the most stable magnetic treatment.²³ In contrast, we studied FM, AFM, and three HC structures and found FM to be

the most stable for the U_{eff} range of 0.0–2.0 eV. Thus, no favorable transition between FM and AFM structures was identified. The starting AFM structure consisting of alternating spin-up and spin-down (100) planes was the least stable after the U-ramp and revealed an entirely new AFM structure. This structure consists of not only spin-up and spin-down (100) planes but also planes with half spin-up and half spin-down electrons on U atoms. The magnetic moments of the U atoms in the FM structure ranged from $1.72 \mu_B$ in the central layers to $2.10 \mu_B$ in the terminating layers. The average magnetic moment of all the U atoms in the FM structure, $1.88 \mu_B$, is in agreement with the $1.89 \mu_B$ value found by Claisse *et al.* for bulk UN.³² While the magnetic moment determined experimentally is $0.75 \mu_B$, Curry theorized this value approaching $3.3 \mu_B$.¹⁵

To determine the effects of magnetic structure on corrosion, OH was optimized at the U-top site for FM, AFM, and NM magnetic structures. Bond lengths, bond angles, and adsorption energies vary by up to 0.05 Å, 17.95°, and 0.82 eV, respectively, across the three magnetic structures. The LDOS shows similar trends across the magnetic structures including valence electrons localized primarily to U from –6 to –2 eV and to N from –2 eV to the Fermi energy. Additionally, hybridization of U and N with O occurs around –4 eV. To identify any differences in the electronic profiles when mapped to the atomic structure, PCD was used to map the states from –6 eV to the Fermi energy and from –2 eV to the Fermi energy. The PCDs for the –2 eV to the Fermi energy

range reveal variations in bond degradation across magnetic structures. In all three magnetic structures, covalent bonding is weakened between U1 and its neighboring U and N atoms as compared to the bulk. However, in FM, the bond between U1 and U2 is weakened to the extent that the contour no longer shows a connecting region. In AFM, the contour no longer shows a connecting region between U1 and N1. NM does not show bond weakening between U1 and its neighboring atoms to the same extent as FM and AFM. These results suggest that each magnetic structure could suggest different corrosion mechanisms when interacting with dissociated water. Key differences in the ELF can be seen between the AFM structure and the other structures. First, there is an unphysical charge build-up next to the pristine surface suggesting metastability. Second, the AFM ELF revealed that more charge is localized to U atoms with spin-down electrons than any other U or N atoms. As such, adsorption properties could vary, depending on if the adsorbates interact with a spin-up or spin-down terminated surface.

Our findings reveal insight into the magnetic structures that could be computationally used when studying UN surfaces. While AFM is the most favorable magnetic structure of bulk UN, FM remains the most favorable magnetic structure of the UN surface with consideration of the Hubbard U-term. DFT studies of AFM UN surfaces should consider both slabs terminated with spin-up electrons and spin-down electrons as this can lead to defect energies varying on the order of 0.27 eV (Table II). Additionally, the AFM structure of bulk UN shown in Fig. 1 was not found to be favorable for a surface. As such, future AFM surface studies should employ a metastability treatment to allow the magnetic structure to optimize to a ground state magnetic configuration. Finally, the NM structure was found to yield similar OH adsorption trends in the LDOS, ELF, and PCD to the FM structure. While the adsorption energy of OH at the NM slab differed from the FM slab by 0.82 eV (Table II), NM studies expect to resolve similar electronic profiles to those of DFT. This is of particular importance for *Ab Initio* Molecular Dynamics (AIMD) studies that would enable investigation of UN corrosion with time and temperature effects and commonly ignore spin polarization. Future computational work studying energetically favorable UN surfaces could reveal more accurate corrosion mechanisms to compare with experiments.

V. CONCLUSIONS

We performed DFT-based electronic structure calculations and found the FM surface to be the most energetically favorable magnetic structure for the U_{eff} range of 0.0–2.0 eV. This reveals that FM treatment can be used in future studies to reveal the most energetically favorable UN corrosion mechanisms. AFM treatment of alternating (100) spin-up and spin-down planes is not a favorable structure after metastability treatment. It would require a consideration of the effects of spin-up vs spin-down electron termination on adsorption properties. FM, AFM, and NM treatments yield varying adsorbate bond angles and adsorption energies. The electronic maps of the three magnetic structures indicate similar corrosion mechanisms even though the finer resolution of bond weakening in the PCD is seen in FM and AFM. This indicates that future AIMD studies investigating UN corrosion with respect to

time and temperature could turn spin consideration off and maintain general electronic profile trends. This work sets a foundation for magnetic treatment in first-principles UN surface studies. The evaluation of DFT and AIMD accuracy in adsorption properties supports future opportunities to corroborate computational and experimental UN corrosion studies.

ACKNOWLEDGMENTS

The authors would like to acknowledge the Center for Advanced Energy Studies for supporting this effort, providing access, and enabling collaboration that otherwise may have been unavailable. This research made use of the resources of the High Performance Computing Center at Idaho National Laboratory, which is supported by the Office of Nuclear Energy of the U.S. Department of Energy and the Nuclear Science User Facilities under Contract No. DE-AC07-05ID14517.

DATA AVAILABILITY

The data that support the findings of this study are available from the corresponding author upon reasonable request.

REFERENCES

- ¹J. Choi, B. Ebbinghaus, T. Meiers, and J. Ahn, *Laboratory Directed Research and Development (LDRD) on Mono-Uranium Nitride Fuel Development for SSTAR and Space Applications* (Livermore, CA, 2006).
- ²Y. Zhukovskii, D. Bocharov, D. Gryaznov, and E. Kotomi, in *Advances in Nuclear Fuel* (InTech, 2012), Chap. 5, pp. 95–122.
- ³J. K. Watkins, A. Gonzales, A. R. Wagner, E. S. Sooby, and B. J. Jaques, *J. Nucl. Mater.* **553**, 153048 (2021).
- ⁴R. M. Dell, V. J. Wheeler, and N. J. Bridger, *Trans. Faraday Soc.* **63**, 1286 (1967).
- ⁵S. Sugihara and S. Imoto, *J. Nucl. Sci. Technol.* **6**, 237 (1969).
- ⁶G. A. R. Rao, S. K. Mukerjee, V. N. Vaidya, V. Venugopal, and D. D. Sood, *J. Nucl. Mater.* **185**, 231 (1991).
- ⁷M. Jolkonen, P. Malkki, K. Johnson, and J. Wallenius, *J. Nucl. Sci. Technol.* **54**, 513 (2017).
- ⁸J. K. Watkins, D. P. Butt, and B. J. Jaques, *J. Nucl. Mater.* **518**, 30 (2019).
- ⁹D. Bocharov, D. Gryaznov, Y. F. Zhukovskii, and E. A. Kotomin, *J. Nucl. Mater.* **416**, 200 (2011).
- ¹⁰D. Bocharov, D. Gryaznov, Y. F. Zhukovskii, and E. A. Kotomin, *J. Nucl. Mater.* **435**, 102 (2013).
- ¹¹R.-S. Li, X. Peng, W. Fei, and M. Wen-Yan, *Nucl. Sci. Technol.* **25**, 050502 (2014).
- ¹²T. Bo, J.-H. Lan, Y.-J. Zhang, Y.-L. Zhao, C.-H. He, Z.-F. Chai, and W.-Q. Shi, *Phys. Chem. Chem. Phys.* **18**, 13255 (2016).
- ¹³T. Bo, J.-H. Lan, Y.-L. Zhao, C.-H. He, Z.-F. Chai, and W.-Q. Shi, *J. Nucl. Mater.* **492**, 244 (2017).
- ¹⁴E. L. Sikorski, T. H. da Silva, L. K. Aagesen, B. J. Jaques, and L. Li, *J. Nucl. Mater.* **523**, 402 (2019).
- ¹⁵N. A. Curry, *Proc. Phys. Soc.* **86**, 1193 (1965).
- ¹⁶Yu. F. Zhukovskii, D. Bocharov, and E. A. Kotomin, *J. Nucl. Mater.* **393**, 504 (2009).
- ¹⁷Yu. F. Zhukovskii, D. Bocharov, E. A. Kotomin, R. A. Evarestov, and A. V. Bandura, *Surf. Sci.* **603**, 50 (2009).
- ¹⁸J. Chen, Z. Long, R. Qiu, Y. Hu, B. Ao, and K. Liu, *J. Nucl. Mater.* **533**, 152095 (2020).
- ¹⁹S. L. Dudarev, G. A. Botton, S. Y. Savrasov, Z. Szotek, W. M. Temmerman, and A. P. Sutton, *Phys. Status Solidi A* **166**, 429 (1998).
- ²⁰J. Hubbard, *Proc. R. Soc. London A* **276**, 238 (1963).
- ²¹J. Hubbard, *Proc. R. Soc. London A* **285**, 542 (1965).

- ²²Y. Lu, B.-T. Wang, R.-W. Li, H. Shi, and P. Zhang, *J. Nucl. Mater.* **406**, 218 (2010).
- ²³D. Gryaznov, E. Heifets, and E. Kotomin, *Phys. Chem. Chem. Phys.* **14**, 4482 (2012).
- ²⁴D. Bocharov, D. Gryaznov, Y. F. Zhukovskii, and E. A. Kotomin, *Surf. Sci.* **605**, 396 (2011).
- ²⁵D. Rafaja, L. Havela, R. Kužel, F. Wastin, E. Colineau, and T. Gouder, *J. Alloys Compd.* **386**, 87 (2005).
- ²⁶E. L. Bright, R. Springell, D. G. Porter, S. P. Collins, and G. H. Lander, *Phys. Rev. B* **100**, 1 (2019).
- ²⁷P. W. Tasker, *J. Phys. C: Solid State Phys.* **12**, 4977 (1979).
- ²⁸G. Kresse and J. Furthmüller, *Phys. Rev. B* **54**, 11169 (1996).
- ²⁹J. P. Perdew, K. Burke, and M. Ernzerhof, *Phys. Rev. Lett.* **77**, 3865 (1996).
- ³⁰B. Dorado, P. Garcia, G. Carlot, C. Davoisne, M. Fraczkiewicz, B. Pasquet, M. Freyss, C. Valot, G. Baldinozzi, D. Siméone, and M. Bertolus, *Phys. Rev. B* **83**, 035126 (2011).
- ³¹B. Meredig, A. Thompson, H. A. Hansen, C. Wolverton, and A. Van De Walle, *Phys. Rev. B* **82**, 195128 (2010).
- ³²A. Claisse, M. Klipfel, N. Lindbom, M. Freyss, and P. Olsson, *J. Nucl. Mater.* **478**, 119 (2016).
- ³³R. A. Evarestov, A. V. Bandura, M. V. Losev, E. A. Kotomin, Y. F. Zhukovskii, and D. Bocharov, *J. Comput. Chem.* **29**, 2079 (2008).
- ³⁴A. Savin, R. Nesper, S. Wengert, and T. E. Fassler, *Angew. Chem. Int. Ed.* **36**, 1808 (1997).